# Mimicking natural antioxidant systems for improved photostability in wide bandgap perovskite solar cells

Francesco Bisconti, Mauro Leoncini, Salvatore Gambino, Nadir Vanni, Sonia Carallo, Francesca Russo, Vincenza Armenise, Andrea Listorti, Silvia Colella, Salvatore Valastro, Alessandra Alberti, Giovanni Mannino, Aurora Rizzo

PUBLISHED IN: ACS Nano, Volume 89, Part B, 2021
CITE AS: Francesco Bisconti, Mauro Leoncini, Salvatore Gambino, Nadir Vanni, Sonia Carallo, Francesca Russo, Vincenza Armenise, Andrea Listorti, Silvia Colella, Salvatore Valastro, Alessandra Alberti, Giovanni Mannino, and Aurora Rizzo, *ACS Nano* **2024** *18* (2), 1573-1581

DOI: 10.1021/acsnano.3c09437

URL: https://pubs.acs.org/doi/10.1021/acsnano.3c09437

PUBLICATION DATE: December, 29th 2023

DOCUMENT VERSION: Accepted Manuscript

# Mimicking natural antioxidant systems for improved photostability in wide bandgap perovskite solar cells

*Francesco Bisconti,[1*] Mauro Leoncini,[1,2] Salvatore Gambino,[1] Nadir Vanni,[1,2] Sonia Carallo,[1] Francesca Russo,[3,4] Vincenza Armenise*,[3] *Andrea Listorti,[3] Silvia Colella,[5] Salvatore Valastro,[6] Alessandra Alberti,[6] Giovanni Mannino[6], Aurora Rizzo[1*]*

1 CNR NANOTEC – Istituto di Nanotecnologia, c/o Campus Ecotekne, Via Monteroni, 73100 Lecce, Italy;

2 Dipartimento di Matematica e Fisica "E. De Giorgi", Università del Salento, Campus Ecotekne, via Arnesano, 73100 Lecce, Italy;

3 Dipartimento di Chimica, Università di Bari, Via Orabona 4, 70126 Bari, Italy;

4 Dipartimento di Ingegneria Elettrica e dell'Informazione, Politecnico di Bari, Via Orabona 4, 70126 Bari, Italy

5 CNR NANOTEC – c/o Dipartimento di Chimica, Università di Bari, Via Orabona 4, 70126 Bari, Italy;

6 CNR-IMM, Ottava strada 5 (Zona industriale), 95121 Catania, Italy.

***Corresponding authors: francesco.bisconti@nanotec.cnr.it; aurora.rizzo@nanotec.cnr.it**

## Abstract

Fostered by top power conversion efficiencies (PCEs) of lab-scale devices, industrialization of perovskite solar cells is underway. Nevertheless, intrinsic poor stability of these materials still represents a major concern. Herein, inspired by Nature, the use of β-carotene in perovskite solar cells is proposed to mimic its role as a protective pigment, as occurs in natural photosynthesis. Laser-Mediated Photo-Stability (LMPS) assessment, Fourier-transform infrared spectra analysis acquired in attenuate total reflectance (ATR-FTIR), Spectroscopy Ellipsometry (SE) and Time-Resolved Photoluminescence (TRPL) measurements under stress conditions prove that the inclusion of a thin β-carotene interlayer promotes an high improvement in the photostability of the perovskite films against photooxidation. Importantly, this is accompanied by an improvement of the solar cells PCE that approaches 20 % efficiency with no hysteresis, which is among the highest values reported for mixed halide (I-Br) perovskite with a band gap of 1.74 eV, relevant for coupling with silicon in tandem cells.

**Keywords:** Perovskite, stability, β-carotene, bio-inspired, PSC, solar cells

**TOC**

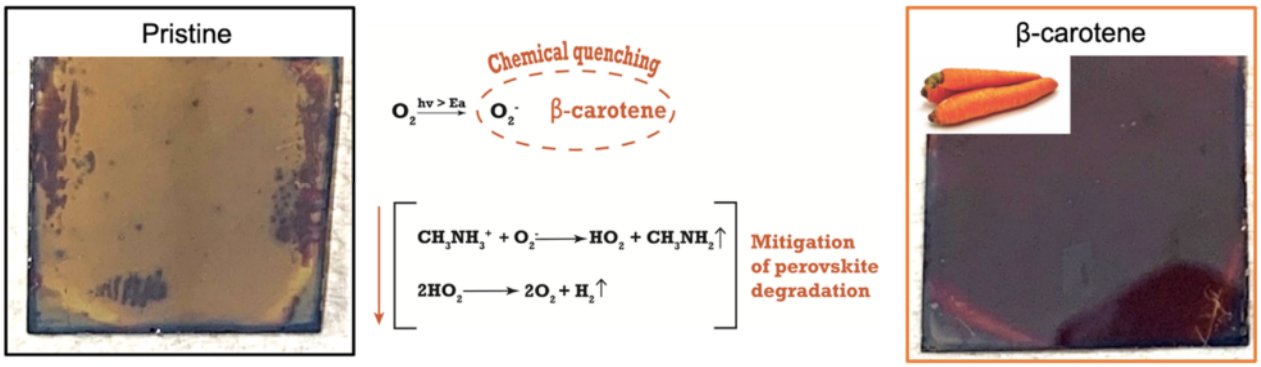


## Introduction

Perovskite solar cells (PSCs) have the potential to be a key player among the photovoltaic technologies of the future. The great potential of perovskite resides in the useful physical properties that allowed it to reach impressive power conversion efficiencies (PCEs) above 25% for lab-scale based devices, in a very brief timeframe following their introduction in the field.[1–5] Perovskite technology also attracts the interest of the industry thanks to the convenient solution processability which is compatible with roll-to-roll printing techniques, and the possibility to develop semi-transparent devices for aesthetic integration in buildings facades.[6–13] Therefore, a growing interest of the scientific community and industrial funding is devoted to the development of standalone PSCs or perovskite-based tandem solar cells with the target of improving their stability and performance.

In general, tandem solar cells are made by pairing two or more different solar cells with complementary absorption to maximise the sunlight harvesting capability. Paring perovskite and silicon technology holds the promise to overcome the Shockley-Queisser (S-Q) limit and finally boost the PCE above 30%.[14] Importantly, the easy compositional tunability of perovskite can be exploited to widen its bandgap, reaching values in the range of 1.7-1.8 eV which is ideal to complement the bandgap of crystalline silicon.[15–19] Among the different strategies to obtain the fine-tuning of the perovskite Energy gap (Eg), varying the halogen ratio, e.g. iodine/bromine ratio in the benchmark $MAPb(I_{1-x}Br_x)_3$ perovskite, it is possible to modulate the bandgap from 1.55 to 2.3 eV.[20–22] Despite the relative simplicity of achieving the desired value of bandgap and besides the halide segregation phenomenon induced by light irradiation, the mixed halide perovskite materials still suffer of stability issue related to different factors like oxygen, moisture, light, elevated temperature, or their synergic effect which need to be urgently solved.[23–28] To overcome or mitigate the stability issue, different approaches have been proposed. Some of them rely on the development of coating materials for the entire device structure, while most of the published work is related to the use of small molecules and

polymers as additives, inside the perovskite structure or at the interface between the perovskite film and the underneath or the above hole-/electron- transporting material.[30–40]

Herein, we propose an innovative approach inspired by Nature to protect the perovskite material from the synergic detrimental effect of light and air. Briefly, plants possess different classes of photosynthetic pigments belonging to the class of chlorophylls and carotenoids useful for better harvesting of the solar spectrum but also to reduce the photooxidation damage that physiologically occurs during the photosynthetic process.[40] Beta carotene (β-carotene) is a compound of the carotenoids group that plays a key role against oxidant species like superoxide, $O_2^-$, and its beneficial activity is studied and exploited in the context of human health.[41] Hence, considering that the metal halide perovskite degradation is triggered by $O_2^-$ [42], we take advantage of the well-known activity of β-carotene against this radical species to protect the perovskite layer. Here we demonstrate that the use of this antioxidant pigment as interlayer in PSC architecture, effectively mitigates the perovskite degradation.

## Results

### Morphological analysis

To exploit the β-carotene activity (molecular structure in Fig. 1a) aiming at the perovskite protection, we took into consideration its solubility in non-polar solvents like toluene and chlorobenzene,[43] orthogonal to the perovskite, deciding to test two different approaches for integration in a p-i-n PSC device architecture: i) the use of β-carotene as an interlayer between the hole extracting layer and the perovskite (hereinafter referred as "β-filter"); ii) the addition of β -carotene in the toluene antisolvent used for the deposition of the perovskite (hereinafter referred as "β-antisolvent"). The device architecture and relative fabrication are reported in the experimental section but, briefly, is based on a self-assembly monolayer (SAM) as hole extracting layer like [2-(9H-Carbazol-9-yl)ethyl]phosphonic acid, 2PACZ, a $MAPb(Br_{0.2}I_{0.8})_3$ perovskite and PC60BM as ETL and bathocuproine (BCP) as hole blocking layer. In Fig. 1b a digital picture of a β-antisolvent perovskite deposited on 2PACZ.

Assumed that $MAPb(Br_{0.2}I_{0.8})_3$ formulation is generally used to obtain a perovskite with an Energy Gap (Eg) that is also compatible with a tandem application, we analysed the absorption spectra and by Tauc Plot equation we estimated the optical Eg of our perovskite, which resulted close to that reported in literature (≅ 1.74 eV)[44] and with a negligible influence of the β-carotene in the band-gap (Fig. S1). Then, morphological, and crystallographic analyses to evaluate the impact of the β-carotene

on the perovskite films were conducted. It is interesting to note how the β-carotene introduction, in comparison to a pristine reference perovskite film (Fig. 1c-d), influences the morphology allowing a more uniform and compact film for both the β-filter and β-antisolvent approach (Fig. 1e-f and Fig. 1g-h, respectively), which is known to be a relevant parameter affecting the overall photovoltaic performance.[45,46] The good quality of the perovskite developed with the β-antisolvent and β-filter approaches was also confirmed by X-ray diffraction analysis showing a complete crystallization process with sharp peaks characteristic of perovskite materials (Fig. S2).

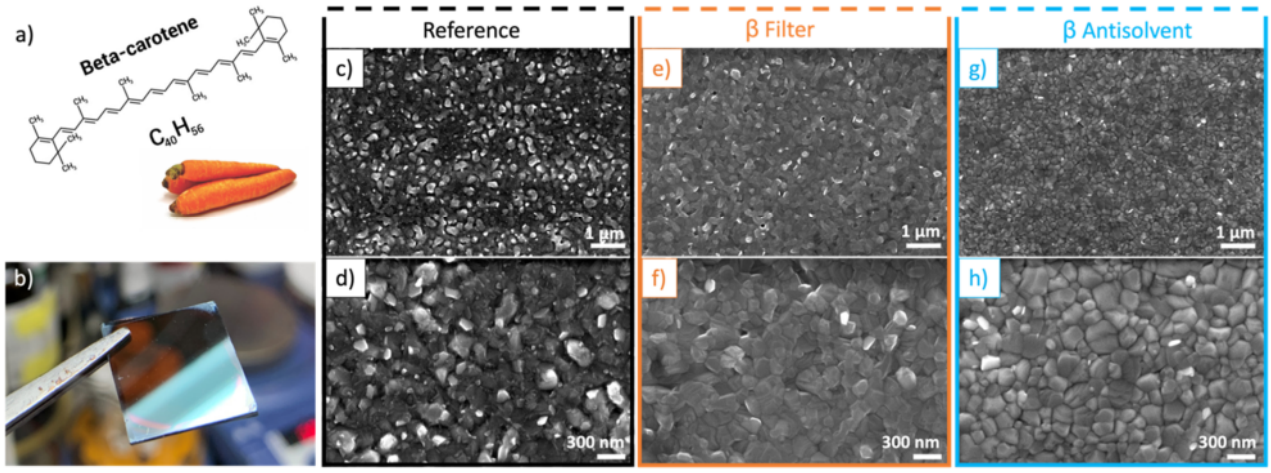


**Fig. 1 Morphological analysis.** a) Molecular structure of β-carotene; b) digital picture of β-carotene modified perovskite film; SEM images of: Reference perovskite film at c) low and d) high magnification, β-filter perovskite at e) low and f) high magnification and β-antisolvent perovskite at g) low and h) high magnification.

## Laser-Mediated Photo-Stability

Assessed the quality of the perovskite films, we evaluated their stability under stress conditions via a Laser-Mediated Photo-Stability (LMPS) assessment. The perovskite films were exposed (3 $mm^2$) at a wavelength of 500 nm by a pulsed laser source with a frequency of 20 Hz, width of 7 ns and average power of 8.4 mW in ambient conditions, without encapsulation. The samples were irradiated for 2 hours, and photoluminescence (PL) spectra acquired every 20 minutes, by exciting the samples at 430 nm with a power intensity of 2.4 mW. The PL spectra analysis revealed a huge difference between the reference perovskite and perovskite samples based on β-carotene. In particular, the reference samples showed a strong and irreversible blueshift of the PL emission peak (Fig. 2a). This behaviour, reported for perovskite nanocrystals and for bulk perovskite,[39,47] it is consequence of the different nature of Pb-I and Pb-Br bonds. The Pb-I bond is longer and weaker than the Pb-Br bond, so is more susceptible resulting in the formation of bromine-rich optical emitters. In the presence of β-carotene, used as a filter or as an antisolvent, the perovskite is protected, in fact, the PL blueshift is remarkably reduced (Fig. 2b-c). The β-carotene possesses a chemical structure rich in double bonds C=C, which

play a central role in the protection against photooxidation,[48] leading, in this context, to better stability of the perovskite material when exposed to laser irradiation in ambient air.

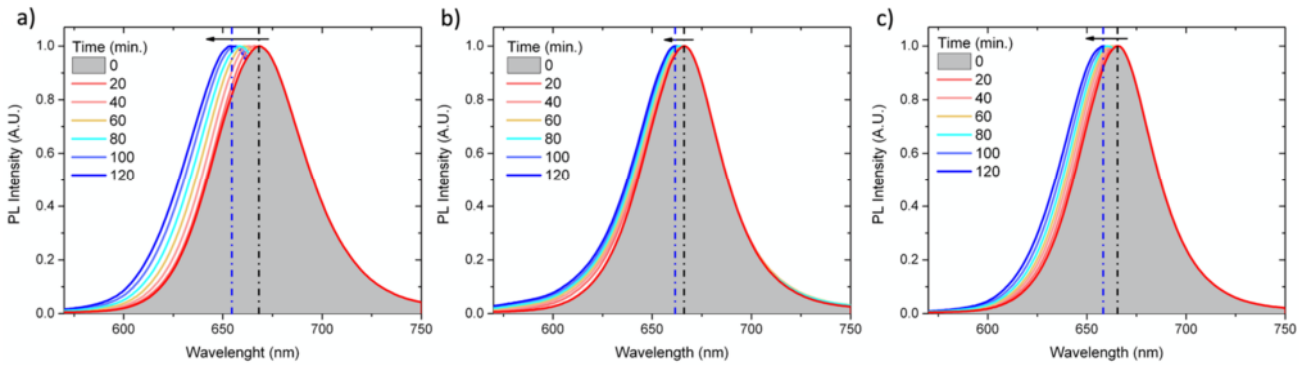


**Fig. 2. LMPS.** Laser mediated photo-stability analysis of a) Reference, b) β filter and c) β antisolvent perovskite under a 500 nm pulsed laser with PL spectra acquired at steps of 20 minutes.

## Fourier-transform infrared spectra, Spectroscopic Ellipsometry and Time-Resolved Photoluminescence

To further study and validate our approach, we carried out a different stress test, characterized by the exposure of perovskite films to a strong oxidant environment, rich in ozone ($O_3$) and $O_2^-$, and evaluating the impact on the perovskite samples by Fourier-transform infrared spectra, acquired in Attenuate Total Reflectance mode (ATR-FTIR), Spectroscopic Ellipsometry (SE) and Time-Resolved Photoluminescence (TR-PL). To the scope, we adapted a UV-Light bromograph exposing the samples to the treatment (below defined as UVO treatment), which resulted subjected to the contextual effect of UV, $O_3$ and $O_2^-$. It has been recently elucidated how these conditions lead to perovskite material degradation. When $CH_3NH_3PbI_3$ perovskite is illuminated in oxygen atmosphere the degradation is swift since $O_2^{\bullet-}$ acts as catalyst deprotonating $CH_3NH_3^+$. The resulting products are $CH_3NH_2$ and hydroperoxyl radical ($HO_2^{\bullet}$). Methylamine is highly mobile molecule at room temperature and diffuse out of the samples, $HO_2^{\bullet}$ decomposed in $H_2$ and $O_2$.[42,49]

The degradation process can be monitored via ATR, signal related to $NH_3^+$ stretching and bending will decease as the methylammonium is lost. Comparing the ATR-FTIR of fresh samples and those subjected to the stress tests for 165 min, it is evident that the intensity of the band corresponding to the asymmetric 3184 $cm^{-1}$ and symmetric 3139 $cm^{-1}$ vibrational stretching of $NH_3^+$ decreases rapidly in the case of the reference (Fig. 3a) compared to the ones including β-carotene (Fig. 3b-c). The signal loss confirms the extraction of a proton from the methylammonium cation by superoxide radicals ($O_2^{\bullet-}$), resulting in the formation of the hydroperoxyl radical ($HO_2^{\bullet}$). The percentage decrease of the area, from 0 min. to 165 min. of stress test, beneath the asymmetric and symmetric vibrational

stretching of $NH_3^+$ signals, were calculated for all samples, resulting in 94%, 68% and 77% for the reference, β-filter and β-antisolvent, respectively. Furthermore, the peaks of symmetric 1469 $cm^{-1}$ and asymmetric 1579 $cm^{-1}$ vibrational bending after 165 minutes of test, are much less reduced in the case of the β-antisolvent and β-filter compared to the reference.

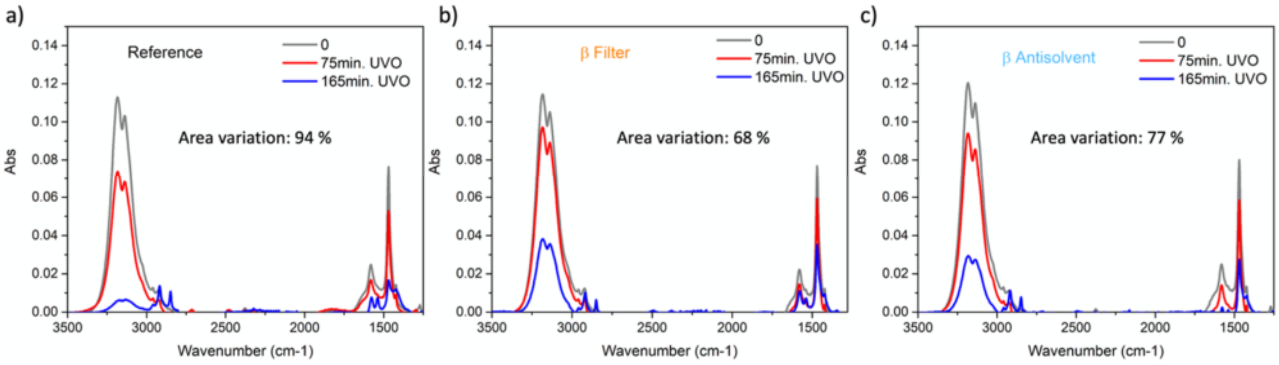


**Fig. 3: ATR-FTIR analysis.** Spectra and area percentage reduction of a) reference, b) β-antisolvent and c) β-filter films deposited on glass exposed to UVO for 0, 75 and 165 min.

Herein, the presence of β-carotene played a key role in mitigating perovskite degradation playing its role as a chemical quencher (Fig. 4a). Ellipsometry data were collected at different angles below and above the Brewster angle of the glass substrate, over a wide range of wavelengths 190–1750nm (0.71-6.5 eV) with a step of 10 nm. The optical model is a three-layer model that considers the optical constants of the glass substrate, the perovskite film and the surface layer needed to simulate the layer roughness. Within the effective model approximation, this last layer was assumed to be made 50% of the upper layer (air) and 50% of the lower layer (perovskite). The presence of a transparent substrate had been properly considered, including the possibility that part of the light hits the back surface of the glass slide. We built a Kramers–Kronig consistent optical model based on multiple critical points parabolic band (CPPB) oscillators to fit experimental data and determine the real and imaginary part of the dielectric function.[50,51] The absorption coefficient can be calculated from the dielectric function according to the equation:

$$\alpha = \frac{2\omega}{c}\sqrt{\frac{\sqrt{(\varepsilon_1^2+\varepsilon_2^2)}-\varepsilon_1}{2}} \qquad \text{Eq. 1}$$

where $\varepsilon_1$ and $\varepsilon_2$ are obtained from the optical model, ω is the frequency of the light and c is the speed of light.

In Fig. 4b we reported the absorption coefficients for reference and β-carotene modified perovskite films. The profile was characterised by the main absorption edge at 1.74eV (the energy gap) and the other two transitions at 2.94eV and 3.43eV. With increasing time, the exposure to the strong oxidant environment produced a clearly visible blue shift in the energy gap (numerical values in Table 1). However, after 160 min of UVO treatment, the absorption edge of reference and β filter perovskite vanished and was replaced by a smooth increase with a long tail, which is a typical marker of a degradation ongoing process (see also insets in Fig. 4b). On the contrary, β antisolvent perovskite showed a negligible shift of +0.04eV with a gap edge still well defined, as a demonstration of a superior resistance of the perovskite material to the stress.

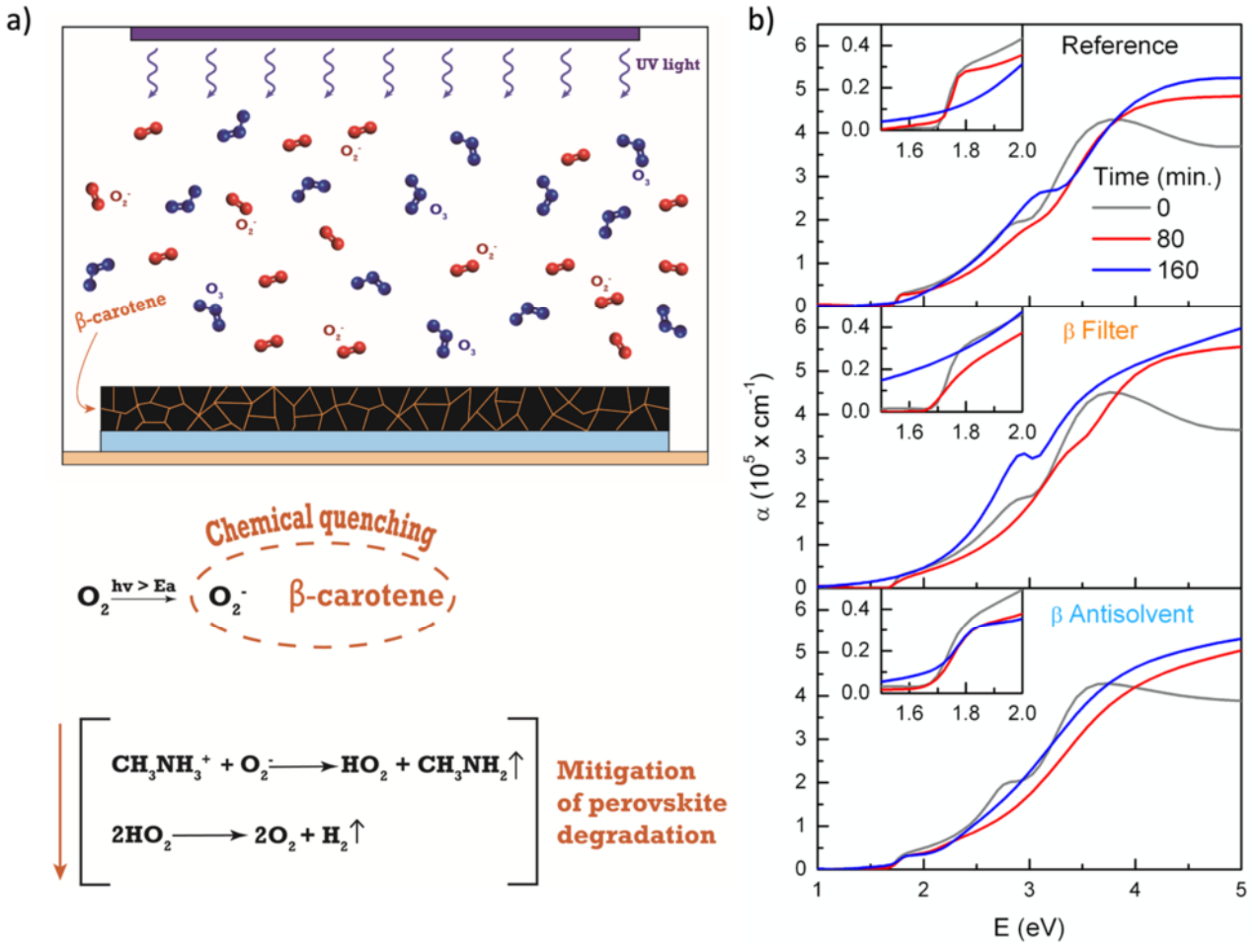


**Fig. 4. Stress test and Spectroscopic ellipsometry.** Schematic illustration of the a) UVO treatment simulating a strong oxidant environment and b) results of the spectroscopic ellipsometry conducted on the samples.

**Table 1.** Value of the Energy Gap for the Reference, β Filter and β Antisolvent perovskite as a function of time.

| Time (min.) | Eg (eV) | | |
|---|---|---|---|
| | Reference | β Filter | β Antisolvent |
| **0** | **1.745** | **1.741** | **1.737** |
| 40 | 1.748 | 1.747 | 1.743 |
| 80 | 1.757 | 1.756 | 1.749 |
| 120 | 1.784 | 1.771 | 1.758 |
| **160** | **1.884** | **1.835** | **1.789** |

Further, measurements of TR-PL were conducted to probe the carrier lifetime of the reference, β-filter and β-antisolvent perovskites with the precise goal of evaluating the optical quality of the different perovskite films after the exposure to oxidant agents.

In Fig. 5 the time-resolved PL spectra of the samples at 0 min, after 75 min, and 165 min of UVO treatment were reported. In the case of the reference perovskite, a reduction of the lifetime just after 75 min was evident, and a rapid fall after 165 min (Fig. 5a). Noteworthy, the results were completely different for the β-filter and for the β-antisolvent perovskite films. The β-filter perovskite showed a slightly longer TRPL signal after 75 min of exposure (Fig. 5b) if compared to the reference, but a rapid decline comparable to the reference after 165 min. This result could be explained since the β-carotene is positioned underneath the perovskite film and, therefore, cannot protect the surface of the perovskite film from oxidating agents. By contrast, noticeably outcome was observed exploiting the β-antisolvent approach. After 165 min of continuous UVO stress test (Fig. 5c), this perovskite still exhibited a strong resistance, with optical properties that were minorly altered as evidenced by TR-PL decay.

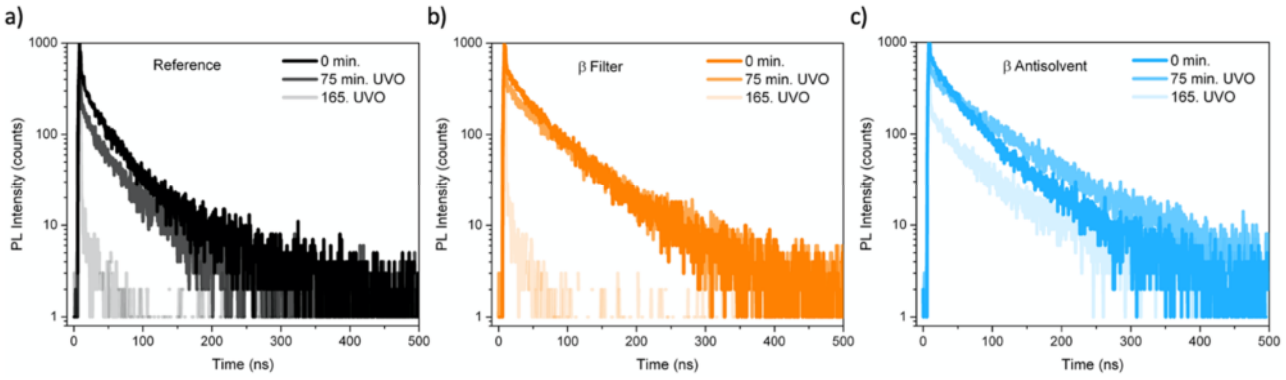

**Fig. 5. TRPL and decays analysis conducted throughout UVO** a) Reference, b) β-filter and c) β-antisolvent perovskite films PL analysed at 0 minutes, after 75 min. and 165 min. of UVO stress test.

In parallel, we acquired the absorption spectra of the fresh and UV-exposed samples, which were in accordance with the TR-PL measurements. After 165 min of UVO stress test both reference and β-filter perovskite revealed an evident blueshift on the absorption onset and a decreased intensity (Fig. S3a-b, digital photos in the inset), while the β-antisolvent sample remained almost unaltered, demonstrating a clear efficacy of this approach in the improvement of the perovskite stability upon exposure to an extremely oxidising environment (Fig. S3c).

## Device integration

Established the material stability improvement, we proceeded with the device integration to understand if the β-filter and the β-antisolvent approach could be also compatible with the obtainment of high PCE. In fact, good performance were recorded, higher than the reference devices embedding $MAPb(Br_{0.2}I_{0.8})_3$ as summarized in Tab. 2, in which the best performances and the average values from 40 devices are reported.

**Table 2. Photovoltaic performance of p-i-n device based on reference, β-filter and β-antisolvent perovskite**. For each kind of device are reported the average values (first lines) and best performance (second lines). Values from 40 devices of different batches.

| $MAPb(Br_{0.2}I_{0.8})_3$ | **FF** | **Voc (V)** | **Jsc ($mA/cm^2$)** | **PCE (%)** |
|---|---|---|---|---|
| **Reference** | 78 ± 2 | 1.14 ± 0.05 | 18 ± 2 | 16 ± 2 |
| | **81.1** | **1.201** | **18.85** | **18.36** |
| **β Filter** | 78 ± 2 | 1.15 ± 0.03 | 20 ± 1 | 18 ± 1 |
| | **78** | **1.201** | **21.73** | **20.26** |
| **β Antisolvent** | 78 ± 2 | 1.15 ± 0.03 | 20 ± 2 | 17.6 ± 1.3 |
| | **79** | **1.195** | **21.1** | **19.91** |

PCE close to 20% and Voc of 1.2 V are reachable with both the β-antisolvent and β-filter architectures. The values of Voc and FF remain substantially unaltered with the use of β-carotene, while the short circuit currents are higher, as can also be clearly seen from the J-V curves. (Fig. 6a) and as verified by the analysis of the External Quantum Efficiency (EQE) of all samples (Fig. 6b). These higher Jsc values can be attributed to the better morphology of the β-carotene modified perovskite films (Fig. 1c-h), which exhibit large and cohesive grains with reduced pinholes compared to the reference perovskite films. A more uniform and less defective perovskite morphology is known

to be a key factor in suppressing current leakage and therefore improving the Jsc of the resulting solar cells.[52–54]

To the best of our knowledge these, hysteresis free, PCE values are among the highest values reported for mixed halide (I-Br) perovskite with a band gap of 1.74 eV.[55]

Measurements of the maximum power point tracking (MPPT) were also conducted to check the device stability under working operations. β-antisolvent perovskite ensured better performance compared to the reference perovskite, showing also an extraordinary absence of hysteresis (Fig. 6c-d).

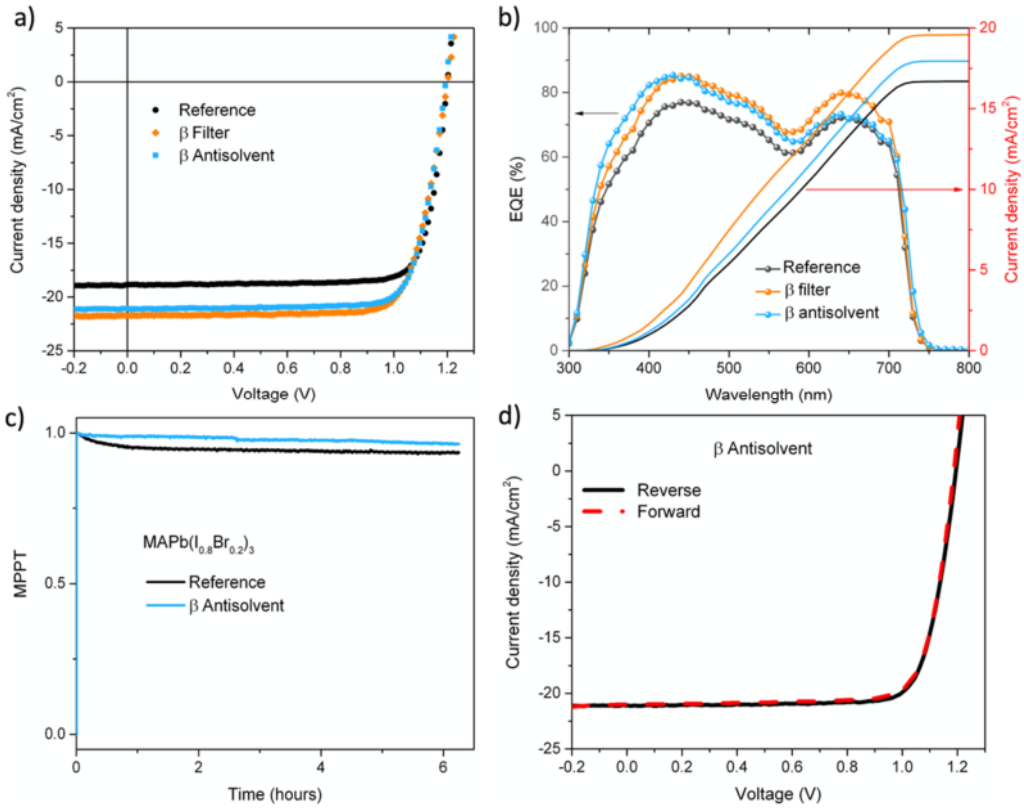


**Fig. 6. Figures of merit of reference and β-modified perovskite solar cells**. a) J-V curves of reference, β-filter and β-antisolvent perovskite-based device acquired in reverse condition and their b) EQE spectra with integrated currents. c) MPPT of reference and β-antisolvent based device. d) J-V scans in both reverse and forward conditions of β-antisolvent.

Furthermore, we tested our approach on a different formulation, $MAPb(Br_{0.3}I_{0.7})_3$, to validate the method. Again, we chose this perovskite considering the more recent attention of the scientific community, and that of the companies, for wide bandgap perovskites suitable for photovoltaic tandem application. Observing the data reported in Tab. S1 it is evident how the presence of the β-carotene interlayer allowed it to reach in this case a slightly higher PCE if compared to the reference devices (18%). Analyzing the average values from 18 devices resulted in a similar trend revealed with

$MAPb(Br_{0.2}I_{0.8})_3$. β-carotene did not afflict negatively the FF and Voc values, in contrast, allowed the achievement of higher values of short circuit current (see also Fig. S4 that reports the characteristic J-V curves of the best performing $MAPb(Br_{0.3}I_{0.7})_3$ reference and $MAPb(Br_{0.3}I_{0.7})_3$ β-antisolvent).

**Conclusion**

Despite the results achieved by the scientific community in terms of power conversion efficiency, the commercialization of perovskite solar cells is hampered for several reasons, such as the poor stability of perovskite materials due to stress factors (oxygen, light, humidity).

With our research work, we proposed an alternative and a very effective approach that mimics what happens in nature, where accessory pigments like β-carotene are fundamental in the photosynthetic process to preserve stability and activity of main pigments (i.e. chlorophyll) of the photoreactive centers. We exploited the scavenging properties of β-carotene to fight the perovskite degradation triggered by oxidant species generated during device operation. We tested the inclusion of this antioxidant species by two different approaches and investigated its influence on the perovskite stability by LMPS assessment, ATR-FTIR, Spectroscopy Ellipsometry and TR-PL after a stress test in a tough oxidant environment. Good results were obtained using the β-antisolvent approach, envisioning the inclusion of β-carotene in the device during the antisolvent step. β-antisolvent perovskite revealed higher stability under LMPS and a better resistance to the oxidant agents, as demonstrated by the analysis of the charge carriers' lifetime and the absorption spectrum by spectroscopic ellipsometry and ATR-FTIR. Once proved the increased stability under harsh conditions, we verified the p-i-n device integration. PCE of around 20 % was obtained in the device built with the β-antisolvent approach, characterized by a high Voc (1.2 eV) and very high short circuit currents if compared to the reference perovskite devices. In conclusion, we demonstrated how to improve perovskite material stability mimicking what occur in natural photosynthesis, making a more robust device without disturbing its photovoltaic performance.

## Methods

### *Materials*

Lead (II) iodide ($PbI_2$, ultradry 99.999 % metals basis) and Methylammonium iodide ($CH_3NH_3I$, MAI) were purchased from Alfa Aesar (Kandel, Germany) and GreatCell Solar, respectively. Dimethyl sulfoxide anhydrous, 99.9 % (DMSO); Toluene anhydrous, 99.8 % (TOL); Chlorobenzene anhydrous, 99.8% (CB); 2-propanol (IPA); Bathocuproine, 96 % (BCP) and Beta-carotene were purchased from Sigma Aldrich. [6,6]-phenyl $C_{61}$ butyric acid methyl ester (PCBM) was purchased from Nano-c. [2-(9H-Carbazol-9-yl)ethyl]phosphonic Acid (2PACZ) was purchased from TCI. All materials were used as received without any further purification.

### *Solutions preparation*

The perovskite solutions were obtained preparing mother solutions of $MAPbI_3$ 1M (MAI:PbI2 = 1:1) and $MAPbBr_3$ 1M (MABr:$PbBr_2$ = 1:1) employing an equivalent molar concentration of DMSO and DMF as solvent, which were then stoichiometrically mixed together for the $MAPb(I_{1-x}Br_x)_3$ formulations [$MAPb(I_{0.8}Br_{0.2})_3$ and $MAPb(I_{0.7}Br_{0.3})_3$]. A 1 mM stock solution of Beta-carotene in toluene was prepared and used depending on the approach.

All solutions were stored in $N_2$ filled glove box after the preparation and covered with aluminum foil.

### *Perovskite film deposition and characterization*

*Perovskite solutions* were deposited by spin coating at 4000 rpm for 25 sec using neat toluene (reference perovskite) or Beta-carotene solution (β-antisolvent perovskite) as solvent dripping and annealed at 100°C for 10 min. For the β-filter approach, the Beta-toluene solution was deposited prior to the perovskite at 4000 rpm for 25 sec and annealed at 100°C for 10 min.

The Scanning Electron Microscopy (SEM) analysis were conducted by Carl Zeiss Auriga40 Crossbeam (Zeiss) instrument in high vacuum and high-resolution mode, equipped with Gemini column and an integrated high efficiency in-lens detector. A 5 kV voltage acceleration was applied.

The *X-Ray Diffraction* (XRD) spectra of perovskite films were measured with a PAN analytical X'Pert-PRO Materials Research Diffractometer using graphite-monochromated CuK α radiation (λ = 1.5405 Å).

The *UVO stress test* were conducted with a homemade setup adapting a UV Light bromograph.

The *absorption spectra* were analyzed by PerkinElmer Spectrophotometer (Lambda 1050) in the 400-800 nm range and the Optical Energy Gap was determined by Tauc Plot method.

*Digital photo* acquired by iPhone XR.

*Laser-mediated photo-stability*: probed by irradiating the sample at a wavelength of 500 nm, by Laser pulses of 7 ns (width) and an average power of 8.4 mW, at a repetition frequency of 20 Hz. Each sample was pumped for 120 minutes. PL spectra were acquired by exciting the sample at a 430 nm, at steps of 20 minutes and at an average light intensity of 2.4 mW. The measurements were conducted at room temperature in ambient air condition.

*ATR-FTIR*: A vacuum Bruker Vertex 70v Fourier transform infrared spectrometer was used to register the infrared absorption spectra of perovskite thin films deposited on glass, in the range 400-4000 $cm^{-1}$ over 32 scans with a resolution of 4 $cm^{-1}$. Spectra were collected in attenuate total reflectance mode utilizing an ATR module equipped with a single reflection diamond ATR crystal (refractive index of 2.4). ATR-FTIR spectra were baseline corrected.

For Spectroscopic Ellipsometry was used a V-VASE, J.A. Woollam spectroscopic ellipsometer equipped with an Autotrader for optical characterization.

*TR-PL*: the photoluminescence (PL) measurements were recorded by means of a Fluorolog®-3 spectrofluorometer (HORIBA Jobin-Yvon), equipped with a 450 W xenon lamp as exciting source and double grating excitation and emission monochromators. All the optical measurements were performed at room temperature on thin film deposited on glass. The PL emission spectra were recorded by using an excitation wavelength of 375 nm. The spectrofluorometer was equipped with a FluoroHub (HORIBA Jobin-Yvon) module to perform lifetime measurements by Time-Correlated Single Photon Counting (TCSPC) technique. The pulsed excitation source was a laser diode emitting at 485 nm (NanoLED N485L, pulse width <200 ps, average power of 14pJ/pulse) with a repetition rate of 1 MHz. The PL emission was detected by a picosecond photon counter (TBX ps Photon Detection Module, HORIBA Jobin-Yvon).

***Device fabrication and characterization***

A p-i-n device architecture was developed using 15x15x1.1 mm ITO patterned glass substrates, 2PACZ as hole transporter layer (HTL), perovskite as photoactive layer, PC60BM as electron transporter layer (ETL), BCP as hole extracting layer (HBL) and Ag as cathode top electrode. Except for the Ag all materials were deposited by spin coating in $N_2$ filled Glove Box (< 0.1 ppm [O.2], < 0.1 ppm [$H_2O$]) with the following parameters: 3000 rpm for 30 sec followed by 100 °C x 10 min annealing for 1mM solution of 2PACZ in 2-propanol, a dynamic washing step with 2-propanol and 100 °C x 10 min annealing; perovskite deposition as described above; 1000 rpm for 60 sec for 25 mg/ml Chlorobenzene PCBM solution and 6000 rpm for 20 sec for 0.5 mg/ml 2-propanol BCP solution. 60 nm Ag were thermally evaporated (Lesker Co. instrument) in high vacuum ($5x10^{-6}$ mBar)

as cathode top electrode, with a deposition rate of 0.6 A/s and employing a mask that define a 0.04 $cm^2$ active area.

The photovoltaic device J-V Characteristics were acquired in $N_2$ atmosphere at 25 °C by a Keithley 2400 Source Measure Unit under an irradiation intensity of 100 $mW/cm^2$, employing an Air Mass 1.5 Global (AM 1.5 G) Solar simulator (Newport 91160A, periodically calibrated lamp) and using a black rubber mask to isolate the active area. J-V scan were performed in voltage ranging from 1.2 V to -0.2 V in both reverse and forward direction.

Maximum Power Point Tracking were carried out in glove box under continuous 1 SUN illumination while the External Quantum Efficiency was measured in ambient air condition.

## Supporting information

The Supporting Information is available online.

Energy gap calculation**,** XRD analysis, UVO stress test and absorption spectra, photovoltaic performance of p-i-n device based on reference and β antisolvent $MAPb(Br_{0.3}I_{0.7})_3$ perovskite, J-V curves of reference and β-antisolvent MAPb(Br0.3I0.7)3 perovskite based solar cells. All data are available online.

## References


1. Snaith, H. J. Present status and future prospects of perovskite photovoltaics. *Nat. Mater.* **17**, 372–376 (2018).
2. Mitzi, D. B. Templating and structural engineering in organic–inorganic perovskites. *J. Chem. Soc. Dalt. Trans.* 1–12 (2001) .
3. Huang, Y., Lei, X., He, T., Jiang, Y. & Yuan, M. Recent Progress on Formamidinium-Dominated Perovskite Photovoltaics. *Adv. Energy Mater.* **12**, 1–19 (2022).
4. Li, Z. *et al.* Organometallic-functionalized interfaces for highly efficient inverted perovskite solar cells. *Science (80-. ).* **376**, 416–420 (2022).
5. Ma, F. *et al.* Developments of Highly Efficient Perovskite Solar Cells. Acc. Mater. Res. 4, 8, 716–725 (2023).
6. Galagan, Y. Perovskite Solar Cells: Toward Industrial-Scale Methods. *J. Phys. Chem. Lett.* **9**, 4326–4335 (2018).
7. Park, N. G. Research Direction toward Scalable, Stable, and High Efficiency Perovskite Solar Cells. *Adv. Energy Mater.* **1903106**, 1–14 (2019).
8. Bisconti, F. *et al.* One-step polymer assisted roll-to-roll gravure-printed perovskite solar cells without using anti-solvent bathing. *Cell Reports Phys. Sci.* **2**, 100639 (2021).
9. Bisconti, F. *et al.* Polymer-Assisted Single-Step Slot-Die Coating of Flexible Perovskite Solar Cells at Mild Temperature from Dimethyl Sulfoxide. *Chempluschem* **86**, 1442–1450 (2021).
10. Zuo, L., Shi, X., Fu, W. & Jen, A. K. Y. Highly Efficient Semitransparent Solar Cells with Selective Absorption and Tandem Architecture. *Adv. Mater.* **31**, 1–9 (2019).

11. Rahmany, S. & Etgar, L. Semitransparent Perovskite Solar Cells. *ACS Energy Lett.* **5**, 1519–1531 (2020).
12. Bisconti, F. *et al.* Managing transparency through polymer/perovskite blending: A route toward thermostable and highly efficient, semi-transparent solar cells. *Nano Energy* **89**, 106406 (2021).
13. Pugliese, M. *et al.* Highly Efficient All-Solid-State WO3-Perovskite Photovoltachromic Cells for Single-Glass Smart Windows. *ACS Appl. Energy Mater*. **3**, 11, 10453–10462 (2020).
14. Kabir, E., Kumar, P., Kumar, S., Adelodun, A. A. & Kim, K. H. Solar energy: Potential and future prospects. *Renew. Sustain. Energy Rev.* **82**, 894–900 (2018).
15. Coletti, G. *et al.* Bifacial Four-Terminal Perovskite/Silicon Tandem Solar Cells and Modules. *ACS Energy Lett.* **5**, 1676–1680 (2020).
16. Hossain, M. I. *et al.* Perovskite/perovskite planar tandem solar cells: A comprehensive guideline for reaching energy conversion efficiency beyond 30%. *Nano Energy* **79**, 105400 (2021).
17. Hou, Y. *et al.* Efficient tandem solar cells with solution-processed perovskite on textured crystalline silicon. *Science (80-. ).* **367**, 1135–1140 (2020).
18. Lin, R. *et al.* All-perovskite tandem solar cells with improved grain surface passivation. *Nature* **603**, 73–78 (2022).
19. Zhang, Z., Li, Z., Meng, L., Lien, S. Y. & Gao, P. Perovskite-Based Tandem Solar Cells: Get the Most Out of the Sun. *Adv. Funct. Mater.* **2001904**, (2020).
20. Unger, E. L. *et al.* Roadmap and roadblocks for the band gap tunability of metal halide perovskites. *J. Mater. Chem. A* **5**, 11401–11409 (2017).
21. Noh, J. H., Im, S. H., Heo, J. H., Mandal, T. N. & Seok, S. Il. Nano Lett. 2013, 13, 1764−1769.pdf. *Nano Lett.* **13**, 1764−1769 (2013).
22. Noel, N. K. *et al.* Highly Crystalline Methylammonium Lead Tribromide Perovskite Films for Efficient Photovoltaic Devices. *ACS Energy Lett.* **3**, 1233–1240 (2018).
23. Dunfield, S. P. *et al.* From Defects to Degradation: A Mechanistic Understanding of Degradation in Perovskite Solar Cell Devices and Modules. *Adv. Energy Mater.* **10**, 1–35 (2020).
24. Liu, R., Wang, L., Fan, Y., Li, Z. & Pang, S. UV degradation of the interface between perovskites and the electron transport layer. *RSC Adv.* **10**, 11551–11556 (2020).
25. Heo, S. *et al.* Origins of High Performance and Degradation in the Mixed Perovskite Solar Cells. *Adv. Mater.* **31**, 1–5 (2019).
26. Llacer, J. *et al.* Nanoscale Studies at the Early Stage of Water-Induced Degradation of CH 3 NH 3 PbI 3 Perovskite Films Used for Photovoltaic Applications . *ACS Appl. Nano Mater.* (2020) .
27. Domanski, K., Alharbi, E. A., Hagfeldt, A., Grätzel, M. & Tress, W. Systematic investigation of the impact of operation conditions on the degradation behaviour of perovskite solar cells. *Nat. Energy* **3**, 61–67 (2018).
28. Singareddy, A., Sadula, U. K. R. & Nair, P. R. Phase segregation induced efficiency degradation and variability in mixed halide perovskite solar cells. *J. Appl. Phys.* **130**, (2021).
29. Zhang, H. *et al.* Polystyrene stabilized perovskite component, grain and microstructure for improved efficiency and stability of planar solar cells. *Nano Energy* **43**, 383–392 (2018).
30. Meng, L. *et al.* Improving Photovoltaic Stability and Performance of Perovskite Solar Cells by Molecular Interface Engineering. *J. Phys. Chem. C* **123**, 1219–1225 (2019).

31. Bisconti, F. *et al.* Blocking wide bandgap mixed halide perovskites' decomposition through polymer inclusion. *J. Mater. Chem. C* **11**, 12213-12221 (2023) .
32. Li, Y., Dailey, M., Lohr, P. J. & Printz, A. D. Performance and stability improvements in metal halide perovskite with intralayer incorporation of organic additives. *J. Mater. Chem. A* **9**, 16281–16338 (2021).
33. Xu, H. *et al.* Hydrophobic 2D Perovskite-Modified Layer with Polyfunctional Groups for Enhanced Performance and High Moisture Stability of Perovskite Solar Cells. *Sol. RRL* (2020).
34. Kim, M., Motti, S. G., Sorrentino, R. & Petrozza, A. Enhanced solar cell stability by hygroscopic polymer passivation of metal halide perovskite thin film. *Energy Environ. Sci.* **11**, 2609–2619 (2018).
35. Wang, R. *et al.* Caffeine Improves the Performance and Thermal Stability of Perovskite Solar Cells. *Joule* **3**, 1464–1477 (2019).
36. Huang, T., Tan, S. & Yang, Y. Material, Phase, and Interface Stability of Photovoltaic Perovskite: A Perspective. *J. Phys. Chem. C* **125**, 19088–19096 (2021).
37. Han, T. H. *et al.* Perovskite-polymer composite cross-linker approach for highly-stable and efficient perovskite solar cells. *Nat. Commun.* **10**, 520 (2019).
38. Zuo, L. *et al.* Polymer-modified halide perovskite films for efficient and stable planar heterojunction solar cells. *Sci. Adv.* **3**, 1–12 (2017).
39. Ramasamy, E., Karthikeyan, V., Rameshkumar, K. & Veerappan, G. Glass-to-glass encapsulation with ultraviolet light curable epoxy edge sealing for stable perovskite solar cells. *Mater. Lett.* **250**, 51–54 (2019).
40. Demmig-Adams, B. & Adams, W. W. The role of xanthophyll cycle carotenoids in the protection of photosynthesis. *Trends Plant Sci.* **1**, 21–26 (1996).
41. Pérez-gálvez, A., Viera, I. & Roca, M. Carotenoids and chlorophylls as antioxidants. *Antioxidants* **9**, 1–39 (2020).
42. Nickel, N. H., Lang, F., Brus, V. V., Shargaieva, O. & Rappich, J. Unraveling the Light-Induced Degradation Mechanisms of CH3NH3PbI3 Perovskite Films. *Adv. Electron. Mater.* **3**, 1–9 (2017).
43. Craft, N. E. & Soares, J. H. Relative Solubility, Stability, and Absorptivity of Lutein and β-Carotene In Organic Solvents. *J. Agric. Food Chem.* **40**, 431–434 (1992).
44. Wang, R. *et al.* Prospects for metal halide perovskite-based tandem solar cells. *Nat. Photonics* **15**, 411–425 (2021).
45. Arivunithi, V. M. *et al.* Efficiency Exceeding 20% in Perovskite Solar Cells with Side-Chain Liquid Crystalline Polymer–Doped Perovskite Absorbers. *Adv. Energy Mater.* **8**, 1–8 (2018).
46. Cheng, Y., So, F. & Tsang, S. W. Progress in air-processed perovskite solar cells: From crystallization to photovoltaic performance. *Mater. Horizons* **6**, 1611–1624 (2019).
47. Zhang, H. *et al.* Phase segregation due to ion migration in all-inorganic mixed-halide perovskite nanocrystals. *Nat. Commun.* **10**, 1–8 (2019).
48. Young, A. J. The photoprotective role of carotenoids in higher plants. *Physiol. Plant.* **83**, 702–708 (1991).
49. Siegler, T. D. *et al.* Water-Accelerated Photooxidation of CH3NH3PbI3Perovskite. *J. Am. Chem. Soc.* **144**, 5552–5561 (2022).
50. Valastro, S. *et al.* Black-Yellow Bandgap Trade-Off During Thermal Stability Tests in Low-Temperature Eu-Doped CsPbI3. *Sol. RRL* **6**, (2022).
51. Ceratti, D. *et al.* CsPbBr3, MAPbBr3, and FAPbBr3 bromide perovskite single crystals: Interband critical points

under dry n2 and optical degradation under humid air. *J. Phys. Chem. C* **125**, 4938–4945 (2021).

52. Bae, S., Jo, J. W., Lee, P. & Ko, M. J. Controlling the Morphology of Organic-Inorganic Hybrid Perovskites through Dual Additive-Mediated Crystallization for Solar Cell Applications. *ACS Appl. Mater. Interfaces* **11**, 17452–17458 (2019).
53. Xiao, Z. *et al.* Unraveling the hidden function of a stabilizer in a precursor in improving hybrid perovskite film morphology for high efficiency solar cells. *Energy Environ. Sci.* **9**, 867–872 (2016).
54. Bi, C. *et al.* Non-wetting surface-driven high-aspect-ratio crystalline grain growth for efficient hybrid perovskite solar cells. *Nat. Commun.* **6**, 1–7 (2015).
55. Almora, O. *et al.* Device Performance of Emerging Photovoltaic Materials (Version 3). *Adv. Energy Mater.* **13**, (2023).

## Acknowledgements

This study is a result of the research project “nuovi Concetti, mAteriali e tecnologie per l’iNtegrazione del fotoVoltAico negli edifici in uno scenario di generazione diffuSa” [CANVAS], funded by the Italian Ministry of the Environment and the Energy Security, MASE, through the Research Fund for the Italian Electrical System (type-A call, published on G.U.R.I. n. 192 on 18-08-2022). A. R. gratefully acknowledges the PNRR MUR project: "Integrated Infrastructure Initiative in Photonic and Quantum Sciences" - I-PHOQS (IR0000016) founded by the European Community-Next Generation EU; A. R. and A. G. gratefully acknowledge the project “MISSION INNOVATION, POA 2021-2023 Piattaforma Italiana Accelerata per i Materiali per l'Energia, IEMAP” founded by Italian Ministry of the Environment and the Energy Security, MASE (CUP B82C21001820001). A. R. acknowledges the project Ricerca@Cnr VertiGrow (CUP B15F21004410005). S. C. acknowledges the project Ricerca@Cnr PHOTOCAT (CUP B93C21000060006). A. L. gratefully acknowledges the PRIN 22 and PRIN PNRR 22 projects (REVOLUTION, CUP: 2022HRZH7P and BEAGLE, CUP: P20223HSWX) founded by the European Community-Next Generation EU. S. C. gratefully acknowledges the PRIN 22 and PRIN PNRR 22 projects INTERFACE (2022HWWW3S) and DELPHI (P2022W9773) founded by the European Community-Next Generation EU. A. R. gratefully acknowledges the PRIN 22 and PRIN PNRR 22 projects LEAD-OUT (2022B3C94E) and MASTER (P2022ZYTJY) founded by the European Community-Next Generation EU. We also thank Mario Calora from University of Salento for the support during the device fabrication and for the fruitful discussions.

## Author contributions

**Francesco Bisconti**: Conceptualization, Methodology, Device fabrication and Characterization, Sample preparation for analysis, Writing - original draft preparation, review & editing. **Mauro Leoncini and Salvatore Gambino**: LMPS assessment, Data curation, Writing - review & editing. **Nadir Vanni**: XRD analysis and graphical contents. **Sonia Carallo** SEM measurements. **Salvatore Valastro, Giovanni Mannino and Alessandra Alberti**: Spectroscopic Ellipsometry analysis and data curation. **Francesca Russo:** FTIR samples' preparation and measurements. **Vincenza Armenise:** FTIR measurements and analysis. **Andrea Listorti and Silvia Colella**: TRPL analysis, data curation, Writing - review & editing. **Aurora Rizzo:** Conceptualization, Supervision, Writing - review & editing. All authors discussed the data and commented on the manuscript.

## Competing interests

No competing interests are present.

**Supporting Information**

# Mimicking natural antioxidant systems for improved photostability in wide bandgap perovskite solar cells

*Francesco Bisconti,* [1*] *Mauro Leoncini,* [1,2] *Salvatore Gambino,*[1] *Nadir Vanni,* [1,2] *Sonia Carallo,*[1] *Francesca Russo,*[3,4] *Vincenza Armenise*,[3] *Andrea Listorti,*[3] *Silvia Colella,*[5] *Salvatore Valastro,*[6] *Alessandra Alberti,*[6] *Giovanni Mannino,*[6] *Aurora Rizzo* [1*]

1 CNR NANOTEC – Istituto di Nanotecnologia, c/o Campus Ecotekne, Via Monteroni, 73100 Lecce, Italy;

2 Dipartimento di Matematica e Fisica "E. De Giorgi", Università del Salento, Campus Ecotekne, via Arnesano, 73100 Lecce, Italy;

3 Dipartimento di Chimica, Università di Bari, Via Orabona 4, 70126 Bari, Italy;

4 Dipartimento di Ingegneria Elettrica e dell'Informazione, Politecnico di Bari, Via Orabona 4, 70126 Bari, Italy

5 CNR NANOTEC – c/o Dipartimento di Chimica, Università di Bari, Via Orabona 4, 70126 Bari, Italy;

6 CNR-IMM, Ottava strada 5 (Zona industriale), 95121 Catania, Italy.

***Corresponding authors: francesco.bisconti@nanotec.cnr.it; aurora.rizzo@nanotec.cnr.it**

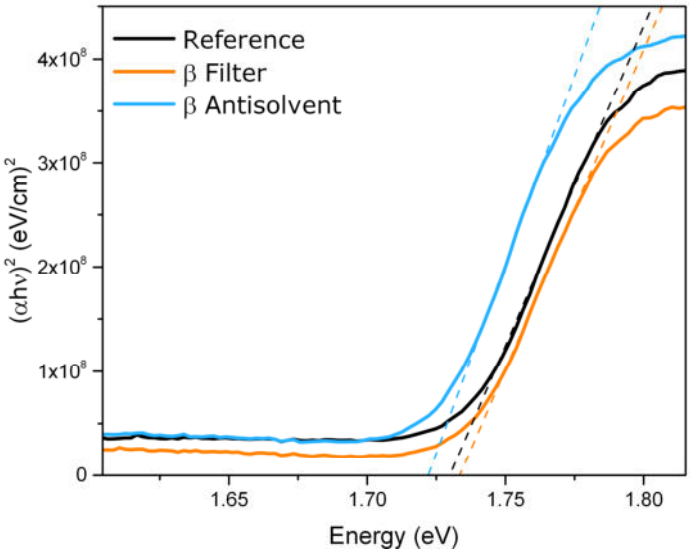


**Fig. S1. Energy Gap calculation.** Tau plot method applied for the estimation of the optical energy gap.

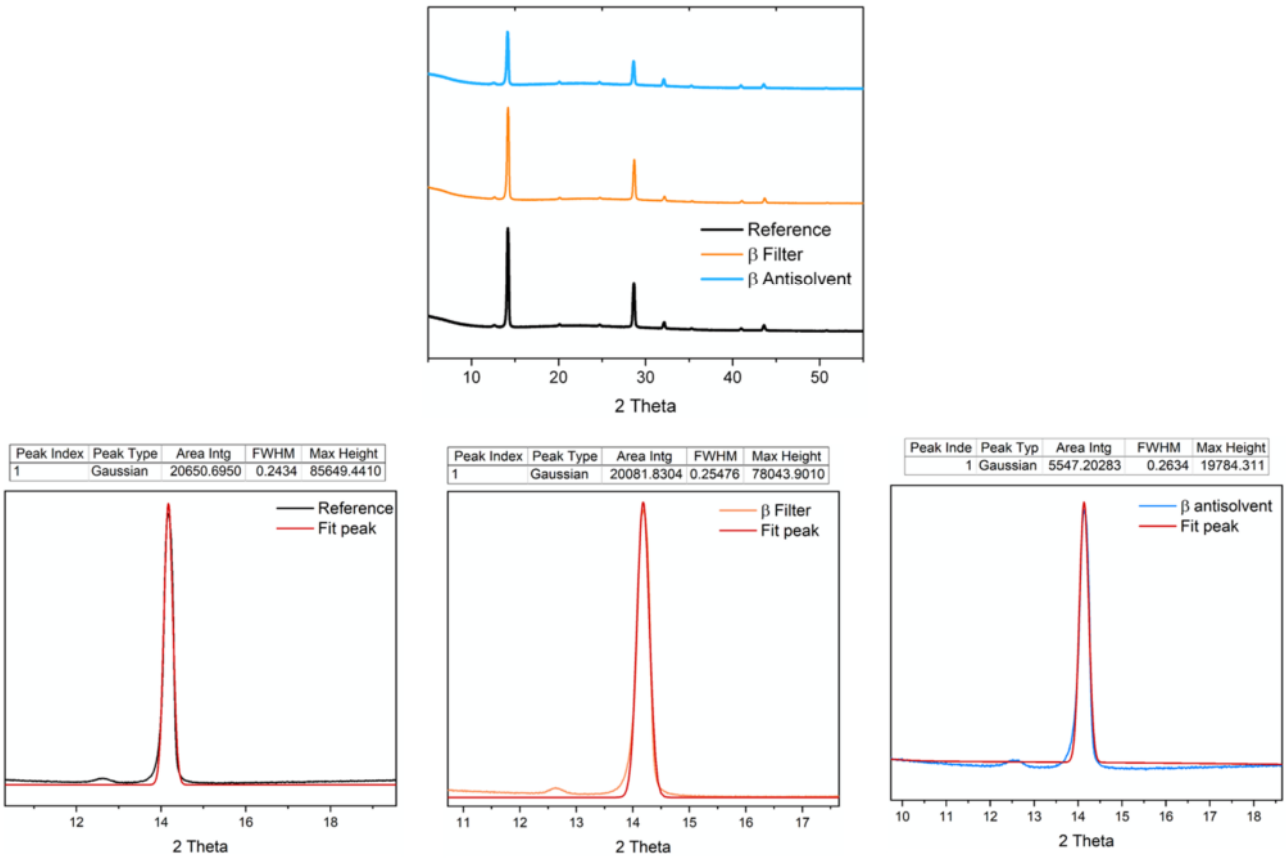


**Fig. S2. XRD analysis.** XRD pattern of reference and β additivated perovskite films.

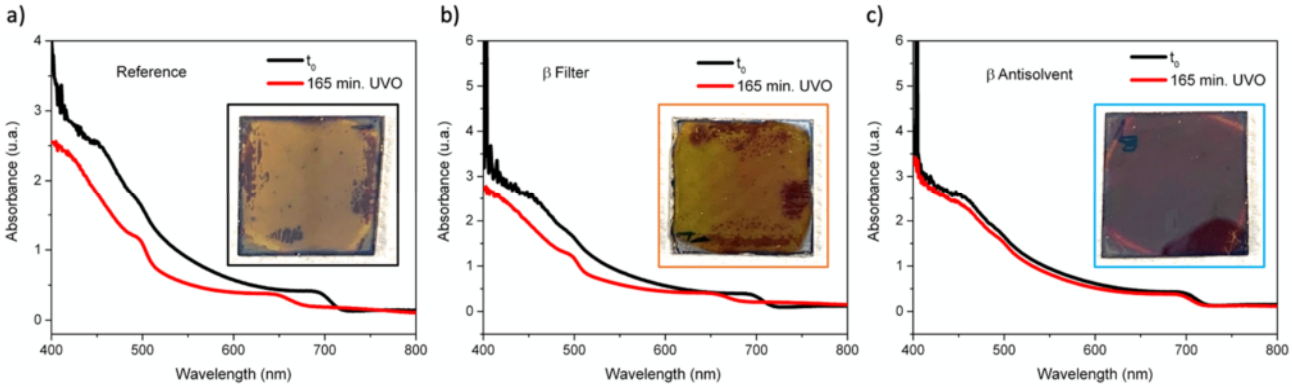


**Fig. S3. UVO stress test and absorption spectra.** a) Reference, b) β-filter and c) β-antisolvent perovskite film absorption before and after 165 min. of UVO treatment. Inset: digital picture of sample at the end of the test.

**Tab S1. Photovoltaic performance of p-i-n device based on reference and β antisolvent $MAPb(Br_{0.3}I_{0.7})_3$ perovskite**. For each kind of device are reported the average values (first lines) and best performance (secondo lines). Values from 18 devices of different batches.

| $MAPbBr_{0.3}I_{0.7}$ | **FF** | **Voc (V)** | **Jsc ($mA/cm^2$)** | **PCE (%)** |
|---|---|---|---|---|
| Reference | 77 ± 3 | 1.14 ± 0.01 | 17 ± 2 | 15 ± 2 |
| | 79 | 1.143 | 19.39 | 17.49 |
| **β Antisolvent** | **78 ± 1** | **1.15 ± 0.01** | **19 ± 1** | **17 ± 1** |
| | **78.3** | **1.153** | **20.37** | **18.4** |

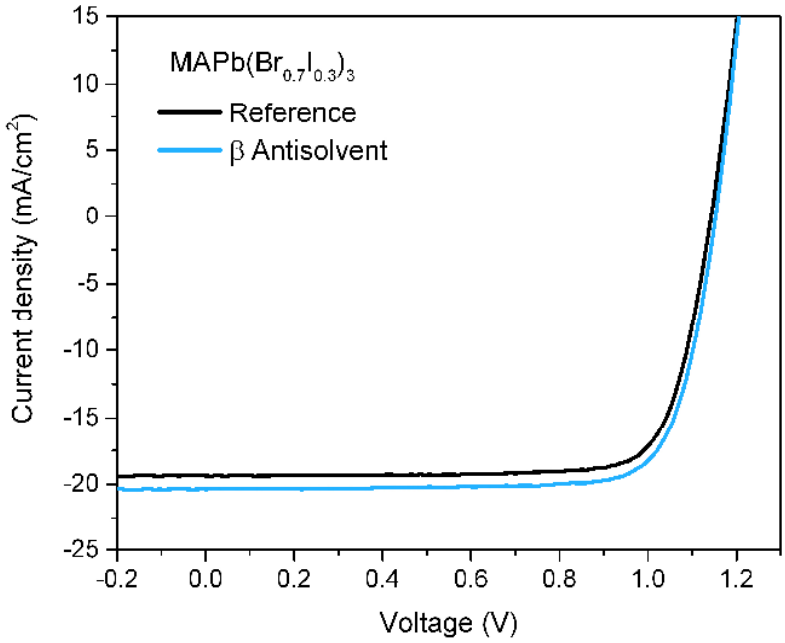


**Fig. S4 J-V curves of reference and β-antisolvent $MAPb(Br_{0.3}I_{0.7})_3$ perovskite based solar cells.**